LETTERS

Single-cell NF-κB dynamics reveal digital activation and analogue information processing

Savaş Tay[1,2]*, Jacob J. Hughey[1]*, Timothy K. Lee[1], Tomasz Lipniacki[3], Stephen R. Quake[1,2] & Markus W. Covert[1]

Cells operate in dynamic environments using extraordinary communication capabilities that emerge from the interactions of genetic circuitry. The mammalian immune response is a striking example of the coordination of different cell types[1]. Cell-to-cell communication is primarily mediated by signalling molecules that form spatiotemporal concentration gradients, requiring cells to respond to a wide range of signal intensities[2]. Here we use high-throughput microfluidic cell culture[3] and fluorescence microscopy, quantitative gene expression analysis and mathematical modelling to investigate how single mammalian cells respond to different concentrations of the signalling molecule tumour-necrosis factor (TNF)-α, and relay information to the gene expression programs by means of the transcription factor nuclear factor (NF)-κB. We measured NF-κB activity in thousands of live cells under TNF-α doses covering four orders of magnitude. We find, in contrast to population-level studies with bulk assays[2], that the activation is heterogeneous and is a digital process at the single-cell level with fewer cells responding at lower doses. Cells also encode a subtle set of analogue parameters to modulate the outcome; these parameters include NF-κB peak intensity, response time and number of oscillations. We developed a stochastic mathematical model that reproduces both the digital and analogue dynamics as well as most gene expression profiles at all measured conditions, constituting a broadly applicable model for TNF-α-induced NF-κB signalling in various types of cells. These results highlight the value of high-throughput quantitative measurements with single-cell resolution in understanding how biological systems operate.

Most of the information on cell signalling has been obtained from population-level studies using bulk assays, yet it is not clear if population data faithfully reflect how individual cells respond[4,5]. For example, pulsed responses of p53 to radiation damage are evident only at the single-cell level[6], and are blurred out in population measurements. Similarly, recent studies of lipopolysaccharide-induced NF-κB activity showed that only half of cells responded to the secondary TNF-α autocrine signal, creating distinct subpopulations[7,8]. Determining variation at the single-cell level is a powerful tool both for understanding drug response[9] and for general understanding of how biological systems work, and single-cell culture measurements often complement *in vivo* studies where cells reside in more complex contexts.

To investigate how individual cells respond to variation in input signal level, we studied nuclear localization dynamics of the transcription factor NF-κB under stimulation with the inflammatory signalling molecule TNF-α. NF-κB controls the expression of hundreds of genes in response to a wide range of stimuli including signalling molecules, and pathogens such as bacteria and virus[10]. The dysregulation of NF-κB is involved in chronic infection, cancer, inflammatory disease, autoimmune disease and improper immune system development[1,11]. Population studies[2] have not revealed the intricate network of information one observes at the single cell level[8,12,13]. Previous time-dependent single-cell experiments were limited to high TNF-α concentrations (10 ng ml^{-1}) and relatively small numbers of cells. Single-cell NF-κB pathway activation and dynamic properties at lower doses have therefore remained an open question.

We cultured 3T3 mouse fibroblast cells[8] in a microfluidic cell culture platform[3] to measure NF-κB activity under ten different TNF-α concentrations (100 ng ml^{-1} to 0.005 ng ml^{-1}) with single-cell resolution (Supplementary Fig. 1). Upon stimulation, NF-κB was transported from the cytoplasm to the nucleus and back out again in characteristic oscillations which we observed with a fluorescent fusion protein (Supplementary Movies 1 and 2). The microfluidic system mimics physiological conditions in terms of volume, fluid flow and number of ligands more plausibly than conventional culture environments where secreted signalling molecules are quickly diluted into millilitres of media. More than 400 live cells were quantified at each condition (Fig. 1) and each experiment was repeated four times, extending the throughput of previous such measurements by more than an order of magnitude (Supplementary Table 1). In parallel experiments with conventional (population based) culture, we used real-time quantitative polymerase chain reaction (qPCR) and digital-PCR to quantify time-dependent expression profiles of 23 target genes under the same concentration range to link NF-κB dynamics to transcriptional activity.

Our measurements reveal the response characteristics of cells at different signal intensities (that is, external TNF-α concentration). One of the most intriguing findings is the discrete nature of single-cell activation: not all cells responded to TNF-α (Fig. 1a, Supplementary Fig. 2 and Supplementary Movies 1 and 2), and the fraction of activated cells decreased with decreasing TNF-α dose (Fig. 1b). Although nearly all of the cells are activated at doses above 0.5 ng ml^{-1}, the percentage of responding cells fell below 50% for 0.1 ng ml^{-1} and fell to 3% at 0.01 ng ml^{-1}. The mean fraction of activated cells of four experiments (N = ~5,000 single cells) is well described by a Hill function with n = 1.5. The activated single-cell traces can be seen in Fig. 1c–f. Notably, the mean area under the first peak for activated cells remained constant over the entire range of concentrations (Fig. 1g), showing that the total NF-κB nuclear activity was equal during the primary response to the signal, indicating digital activation in response to TNF-α. Similarly, the median peak nuclear intensity changed by only a factor of four in response to a four order of magnitude reduction of the TNF-α concentration (Fig. 1h and Supplementary Fig. 3).

To determine whether the heterogeneous cell activation is entirely based on a pre-existing variation in cell sensitivities[14,15] (extrinsic noise[16]), we stimulated the cells with two 20-min-long pulses of intermediate dose (0.1 ng ml^{-1}) TNF-α, while allowing the cells to reset by giving a 180-min break between pulses[13]. Ten per cent of the cells responded to only the first pulse (Fig. 1j), 9% responded to only

[1]Department of Bioengineering, Stanford University, Stanford, California 94305, USA. [2]Howard Hughes Medical Institute, Stanford, California 94305, USA. [3]Institute of Fundamental Technological Research, Warsaw 02-106, Poland.
*These authors contributed equally to this work.

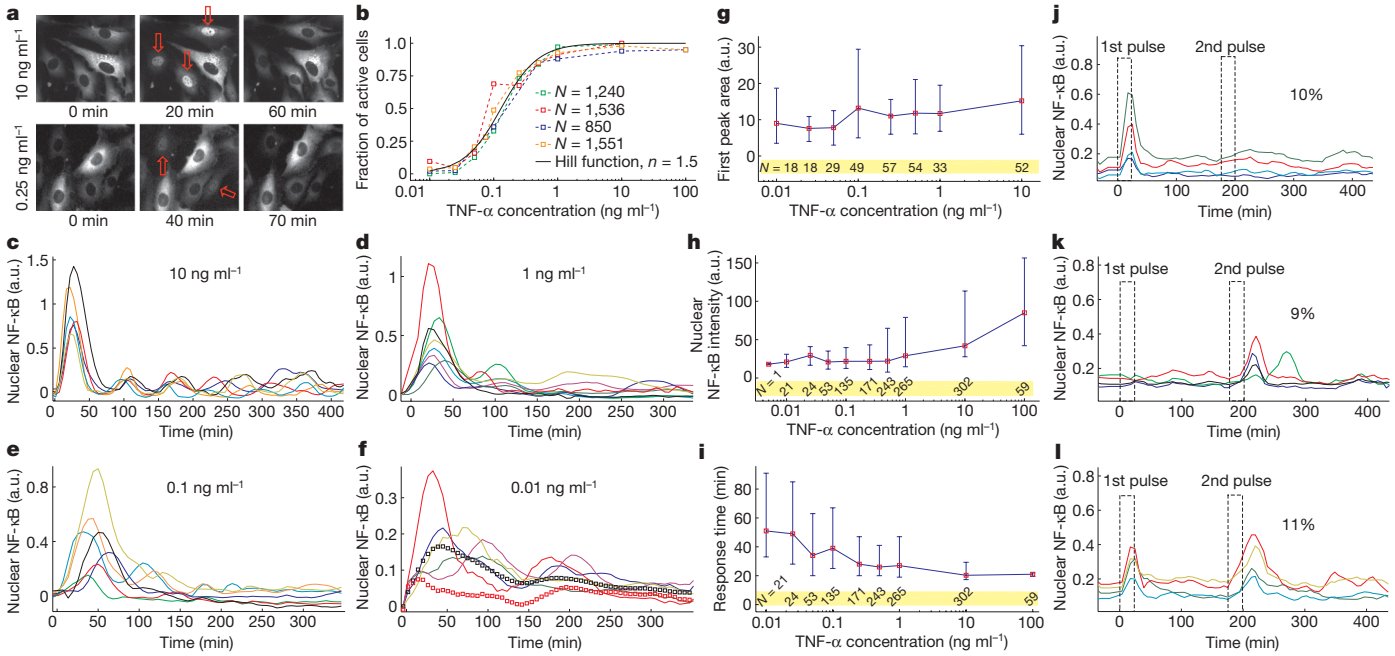

Figure 1 | NF-κB single-cell microscopy measurements. a, Representative real-time fluorescent images of cells during stimulation with 10 ng ml^{-1} (top row) and 0.25 ng ml^{-1} (bottom row) TNF-α. Arrows show the activated cell nuclei. At the high dose, all cells except one respond, whereas only two out of five respond at the lower dose. **b**, Fraction of activated cells versus TNF-α concentration for four different experiments (N = number of quantified active cells). The mean of four experiments fit to a Hill function with $n = 1.5$. **c–f**, Representative traces for active single cells. Also shown (**f**) are population means at 0.01 ng ml^{-1} TNF-α stimulation, when only active cells are included (black squares), and when both active and non-active cells are included (red squares). The population traces averaged over all cells (N = ~80) misleadingly shows reduced activity. **g**, The integrated area under the first peak versus TNF-α concentration for a single experiment, showing that the total NF-κB nuclear activity in the first peak remains constant across all concentrations. **h**, NF-κB nuclear intensity versus TNF-α concentration. **i**, NF-κB response time versus TNF-α concentration. Error bars in **g–i** are the standard deviation from the mean, and show the natural variation in single-cell responses. **j–l**, Representative traces for the low-dose, short-pulsed stimulation experiment. Cells were stimulated with two consecutive 20-min-long pulses of 0.1 ng ml^{-1} TNF-α. The pulses were separated by 180 min, allowing the cells to reset. Ten per cent respond to only the first pulse (**j**), 9% respond only to the second pulse (**k**), and 11% of the cells in the chamber respond to both pulses (**l**). The existence of cells responding to only one of the pulses indicates that NF-κB activation is partly governed by a stochastic process, whereas the high percentage of cell responding to both pulses indicates pre-existing high sensitivity to TNF-α in this subpopulation.

the second pulse (Fig. 1k), and 11% responded to both pulses (Fig. 1l). The existence of cells responding to only one of the pulses shows that the activation is governed partly by a stochastic element. However, the probability of responding to both pulses is highly increased (~10 fold) compared to a purely stochastic process, which suggests that pre-existing variation in internal variables of the cells (extrinsic noise) also has an important role in the outcome[14,15]. The heterogeneous activation of single cells requires the re-interpretation of previous population-level studies[2] and the models derived from them. The population average of only active cells yields an accurate mean nuclear NF-κB intensity (Fig. 1f, black squares). On the other hand, the average over the entire population including active and inactive cells shows significantly reduced mean intensity and completely washed out dynamics (red squares), highlighting the importance of single-cell measurements.

Although the cells show digital activation, there are aspects of their response that are dose-dependent and therefore represent analogue information processing of the stimulus. The cells show significantly delayed activation under lower doses (Fig. 1i). The activation response time (the time from TNF-α stimulation to the first peak) is around 50 min for the lowest doses, whereas the cells activate within 20 min at the highest doses. The variation in response time at the highest doses is close to the experimental resolution of 6 min, and increases to about 60 min at the lower doses. In contrast to the response time, the mean decay time of the first nuclear localization peak (which depends on newly made IκB protein) is around 20 min, and is surprisingly independent of the TNF-α dose (Supplementary Fig. 4).

A related dose-dependent parameter is the number of nuclear oscillations: higher doses yield more oscillations (Supplementary Fig. 5). The intensity of the secondary NF-κB peaks remains relatively constant at high and intermediate doses (Supplementary Fig. 6), but completely disappear in some cells at the lowest doses measured. The time between the first and second peaks remained constant at 80 min over the measured range (Supplementary Fig. 7). Later peaks quickly lose synchrony, and the significant de-phasing after the third peak results in washing-out of the single-cell dynamics at the population level (Supplementary Fig. 3). These subtle variations in the dose-dependent response provide strong constraints on mathematical models of TNF-α-induced NF-κB signalling, which are discussed in more detail below.

At saturating doses of TNF-α, NF-κB nuclear oscillations drive expression of three classes of genes: early, intermediate and late[12,13,17–19]. We measured the time-dependent expression levels of 23 NF-κB target genes on populations of cells from these classes under a broad range of TNF-α doses using qPCR and digital-PCR[20] (Fig. 2 and Supplementary Fig. 8). A series of genes are upregulated at early times, including NF-κB inhibitors *IκBα* (also called *Nfkbia*) and *A20* (also called *Tnfaip3*) (Fig. 2a). Transcripts of early genes often have high degradation rates[18], which resulted in expression profiles that closely follow NF-κB nuclear localization dynamics (Supplementary Fig. 9). An intriguing property of the early-expressed genes is that the expression levels normalized to the fraction of active cells in each population are relatively constant for all doses (Fig. 2b), whereas late genes are only expressed at the highest doses (Fig. 2c). This suggests that the initial NF-κB localization burst is sufficient to express the early genes even at the lowest stimulation doses, linking digital signalling to early gene expression. *IκBα* is one of the digitally expressed genes, which could also explain the dose-independent behaviour of the first peak degradation time we observed in Supplementary Fig. 4.

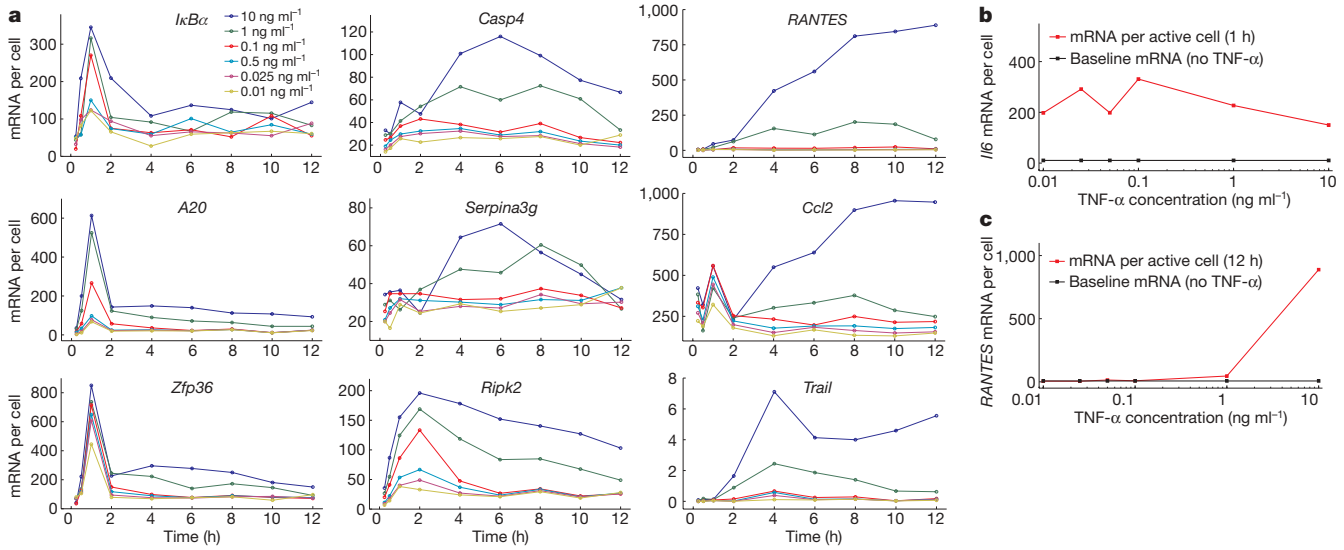

Figure 2 | Time-dependent expression profiles of NF-κB target genes. Cells were stimulated with various doses of TNF-α ranging from 10 ng ml^{-1} to 0.01 ng ml^{-1}. **a**, Relative expression levels of each gene were quantified using approximately 500 cells by qPCR, and digital-PCR was used to calibrate expression levels to the total number of mRNAs per cell. The expression levels shown in **a** are population averages of all cells (active and non-active) in the PCR reaction. Genes cluster in three groups with early (left column), intermediate (middle) and late term (right) activation dynamics. **b**, **c**, Expression levels of a representative early (**b**) and late (**c**) gene normalized to the fraction of active cells at each TNF-α concentration. mRNA levels were normalized to a single active cell level by dividing with the active fraction of cells at that concentration (see Fig. 1). Normalized expression of the early gene *Il6* does not vary in response to a 1,000-fold change in TNF-α concentration. The late gene *RANTES* is expressed only at the highest TNF-α concentrations.

The expression levels of the intermediate and late genes build up slowly after persistent NF-κB oscillations. Such oscillations require constant TNF-α stimulation and thus are observed only when the initial TNF-α level is highest; at low initial concentrations TNF-α quickly disappears from the media due to natural degradation and receptor internalization (Supplementary Fig. 10). The initial localization peak seen in all active cells is not sufficient to induce the late genes (Fig. 2 and Supplementary Fig. 9). Among the late genes that are highly expressed, *Ccl2*, *Trail* (also called *Tnfsf10*), *Casp4*, *Ripk2* and *RANTES* (also called *Ccl5*) lead to apoptotic signalling and *Serpina3g* acts to prevent apoptosis[21]. This suggests that cells that are continuously exposed to high-dose TNF-α activate pro- and anti-apoptotic gene expression programs mediated by late nuclear localization of NF-κB, whereas low-dose TNF-α signals do not lead to apoptosis-related signalling due to a lack of late-term nuclear localization. Furthermore, other signalling molecules and regulatory proteins are also upregulated at early times, including *Il6*, *Ccl20*, *Icam1* and *Zfp36*, suggesting possible synergistic or interfering mechanisms.

The wealth of biochemical data has resulted in a number of mathematical models that describe TNF-α-induced NF-κB nuclear oscillations. Some models are deterministic and therefore unable to reproduce the heterogeneity in single cells[12,17]. Later models incorporate negative regulation of NF-κB by A20[22,23], and use a stochastic description of slow dynamics[24,25]. These models are able to explain the response of the network to repeating short pulses of TNF-α in SK-N-AS cells[13]. Digital cell activation and the overall response characteristics we observed are not simultaneously present in any previous model. We therefore revised the stochastic model[25] to account for our observations. First, we considered the effects of limited TNF-α amount present in the microfluidic chambers and TNF-α degradation on overall TNF-α loss, and included cellular variation in the amount of TNF-α receptor (see Supplementary Mathematical Methods). The resulting model, although more realistic, did not produce the digital activation that we observed at low doses. We therefore implemented a nonlinear IKK (inhibitor of NF-κB kinase) activation profile, where the activation rate of IKK depends quadratically on the concentration of the upstream kinase IKKK. Such a nonlinear activation rate may be justified by the fact that IKK subunits IKK-α and IKK-β must be phosphorylated at two serine residues, S177 and S181, to attain full activity[26]. Incorporation of the quadratic activation resulted in achieving the digital cellular response simulations similar to our experiments (Fig. 3).

The model (Fig. 3a) was manually fitted to the single-cell traces, and a single set of biochemically measured, assumed and fitted parameters were used for all the simulations (see Supplementary Mathematical Methods for model fitting). The core model comprises 16 ordinary differential equations representing biochemical reactions and 34 rate constants, where 20 of the constants are fixed (biochemically measured or based on related data), and the other 14 were varied for model fitting within biologically reasonable boundaries. The internal parameters of the model, such as the number of proteins and mRNAs, production, degradation and transport rates, are all biologically plausible values.

The simulated single-cell traces for 3T3 cells at different TNF-α doses can be seen in Fig. 3c, d and Supplementary Fig. 11, which agree well with the data in terms of timing, intensity and the variability of the first peaks at all doses. Most remarkably, the model can reproduce—within a single set of biochemical parameters—the measured concentration-dependent single-cell activation probability (Fig. 3b), mean nuclear NF-κB intensities (Fig. 3e), the response times (Fig. 3f), and their distributions. Furthermore, it predicts with excellent accuracy the fraction of cells responding to consecutive short pulses of low-dose TNF-α (Fig. 4a). Although the model captures many features of our single-cell microscopy data, it falls short of perfectly reproducing the total number of oscillations at mid doses (Supplementary Fig. 11), first peak decay times and peak-to-peak intensity ratios shown in Supplementary Figs 4–7. Simulated expression profiles for early, intermediate and late genes can be seen in Fig. 4b. The gene expression closely follows NF-κB dynamics and agrees well with most of the genes we measured in Fig. 2. Some measured expression profiles such as *Trail* and *Ccl2* do not follow NF-κB nuclear localization strictly and the single transcription factor model we used was not able to reproduce these profiles, which indicates that parallel synergistic or interfering pathways significantly contribute to transcription of these genes[27].

We have mapped the nuclear localization dynamics of NF-κB under TNF-α stimulation by measuring thousands of single-cell traces and

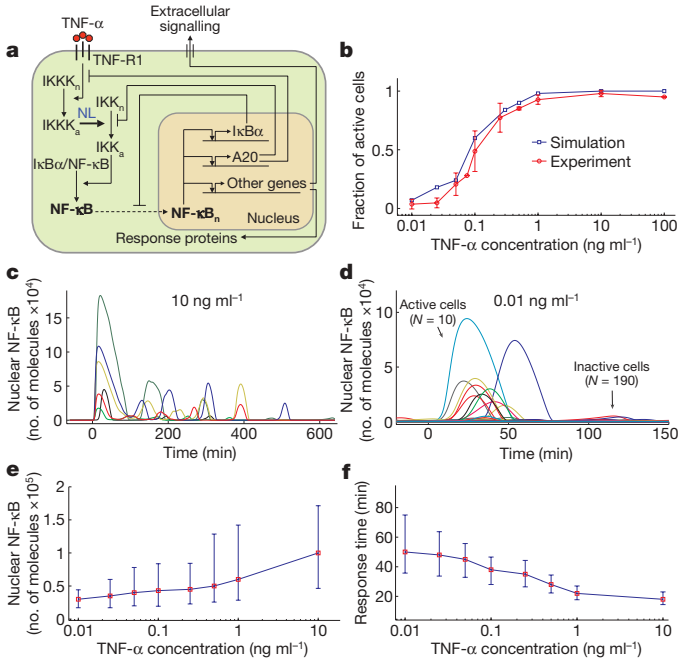

Figure 3 | Mathematical model development and simulations. Where applicable, error bars show standard deviation from the mean. **a**, Model architecture is based on stochastic description of receptor and gene activity, quadratic representation of IKK activation, and negative feedback via IκBα and A20. **b**, Simulated (blue) and measured (red) fraction of activated cells. **c**, **d**, Simulated single-cell NF-κB nuclear localization traces at the experimentally measured TNF-α concentration range. The low dose (0.01 ng ml^{-1}) stimulated cells show clear separation between active and non-active cells similar to experiments. Among 200 simulated cells, only 10 were activated. The model faithfully reproduces important aspects of experimental means and distributions (shown with error bars) across all concentrations. **e**, Simulated NF-κB nuclear intensity versus TNF-α concentration (see Fig. 1h). **f**, Simulated NF-κB response time versus TNF-α concentration (see Fig. 1i).

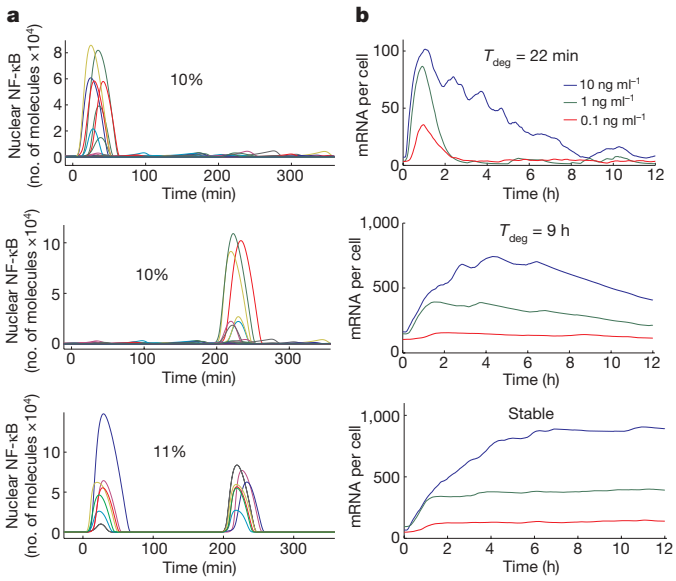

Figure 4 | Model predictions: stochastic and variable cell switching and target gene expression dynamics. **a**, Simulated single-cell traces for low-dose, short-pulsed stimulation. Cells were stimulated with two consecutive 20-min-long pulses of 0.1 ng ml^{-1} TNF-α. The pulses were separated by 180 min. Ten per cent respond to only the first pulse (top), 10% respond only to the second pulse (middle) and 11% of the cells in the chamber respond to both pulses (bottom), showing excellent agreement with experimental results shown in Fig. 1j–l. **b**, Simulations of early (top), intermediate (middle) and late (bottom) term NF-κB target genes under various doses of TNF-α. The model reproduces basic features of the expression profiles shown in Fig. 2a by varying only the transcript degradation times (T_{deg}).

time-dependent gene expression profiles over a concentration range of four orders of magnitude. A mathematical model that reproduces NF-κB dynamics and transcription at the measured concentration range was developed, constituting a significantly improved model of the NF-κB pathway under TNF-α stimulation. We have found that cells activate in response to TNF-α in a digital manner. Although the fraction of activated cells decreases to zero with decreasing TNF-α dose, the NF-κB amplitude remains high, allowing high expression of early genes. Early gene expression is not dependent on the inducing signal intensity, whereas the expression of later genes requires persistent nuclear localizations of the transcription factor, which exist only at the highest input signal levels. The cells process analogue signal intensity information using a diverse set of parameters such as the timing, peak intensity and number of transcription factor oscillations to create digital outputs (activation and early gene expression). In addition to their biological significance, our findings highlight the importance of high-quality, single-cell data in understanding and modelling biological systems, and demonstrate the efficiency of high-throughput microfluidic techniques in obtaining such data.

METHODS SUMMARY

We used a lentiviral system to create *p65*$^{-/-}$ mouse fibroblast (3T3) cells expressing the fluorescent fusion protein p65–DsRed under control of the endogenous mouse *p65* promoter[8]. To relieve a bottleneck in image processing in this study, we also infected the cells with a lentivirus containing the nuclear marker H2B–GFP driven by the human ubiquitin C promoter. Various TNF-α (Roche) dilutions in DMEM were kept on ice at all times and these fluids were flowed into the microfluidic chambers during stimulation. Once the TNF-α media was flowed in, the chambers were sealed and were imaged every 6 min in both GFP and DsRed fluorescence channels, for up to 12 h. For gene expression measurements, we used cells cultured in well plates that were stimulated with different TNF-α concentrations. At the end of each stimulation experiment (0.25, 0.5, 2, 4, 6, 8, 10 and 12 h after stimulation), cells were lysed and cDNA was synthesized using Cells Direct One Step RT–PCR kit (Invitrogen). TaqMan primers and probes (Applied Biosystems) were used for real-time qPCR (Fluidigm 48x48 Dynamic Array). The relative gene expression levels were then calibrated for total mRNA molecules per cell via digital-PCR measurements[20] (Fluidigm 12 Digital PCR Chip). In Fig. 2b, c, we estimate the mRNA levels for only active cells by dividing the expression levels by the fraction of active cells at each dose measured in Fig. 1b.

Full Methods and any associated references are available in the online version of the paper at www.nature.com/nature.

Received 29 December 2009; accepted 28 April 2010.
Published online 27 June 2010.

1. Hayden, M. S., West, A. P. & Ghosh, S. NF-κB and the immune response. *Oncogene* **25**, 6758–6780 (2006).
2. Cheong, R. *et al.* Transient IκB kinase activity mediates temporal NF-κB dynamics in response to a wide range of tumor necrosis factor-α doses. *J. Biol. Chem.* **281**, 2945–2950 (2006).
3. Gómez-Sjöberg, R., Leyrat, A. A., Pirone, D. M., Chen, C. S. & Quake, S. R. Versatile, fully automated, microfluidic cell culture system. *Anal. Chem.* **79**, 8557–8563 (2007).
4. Batchelor, E., Loewer, A. & Lahav, G. The ups and downs of p53: understanding protein dynamics in single cells. *Nature Rev. Cancer* **9**, 371–377 (2009).
5. Spencer, S. L., Gaudet, S., Albeck, J. G., Burke, J. M. & Sorger, P. K. Non-genetic origins of cell-to-cell variability in TRAIL-induced apoptosis. *Nature* **459**, 428–432 (2009).
6. Lahav, G. *et al.* Dynamics of the p53-mdm2 feedback loop in individual cells. *Nature Genet.* **36**, 147–150 (2004).
7. Covert, M. W., Leung, T. H., Gaston, J. E. & Baltimore, D. Achieving stability of lipopolysaccharide-induced NF-κB activation. *Science* **309**, 1854–1857 (2005).
8. Lee, T. K. *et al.* A noisy paracrine signal determines the cellular NF-κB response to LPS. *Sci. Signal.* **2**, 93 (2009).
9. Cohen, A. A. *et al.* Dynamic proteomics of individual cancer cells in response to a drug. *Science* **322**, 1511–1516 (2008).
10. Hoffmann, A. & Baltimore, D. Circuitry of nuclear factor κB signaling. *Immunol. Rev.* **210**, 171–186 (2006).
11. Courtois, G. & Gilmore, T. D. Mutations in the NF-κB signaling pathway: implications for human disease. *Oncogene* **25**, 6831–6843 (2006).

12. Nelson, D. E. *et al.* Oscillations in NF-κB signaling control the dynamics of gene expression. *Science* **306,** 704–708 (2004).
13. Ashall, L. *et al.* Pulsatile stimulation determines timing and specificity of NF-κB-dependent transcription. *Science* **324,** 242–246 (2009).
14. St., Pierre, F. & Endy, D. Determination of cell-fate selection during phage lambda infection. *Proc. Natl Acad. Sci. USA* **105,** 20705–20710 (2008).
15. Snijder, B. *et al.* Population context determines cell-to-cell variability in endocytosis and virus infection. *Nature* **461,** 520–523 (2009).
16. Elowitz, M., Levine, A. J., Siggia, E. D. & Swain, P. S. Stochastic gene expression in a single cell. *Science* **297,** 1183–1186 (2002).
17. Hoffmann, A., Levchenko, A., Scott, M. L. & Baltimore, D. The IκB-NF-κB signaling module: temporal control and selective gene activation. *Science* **298,** 1241–1245 (2002).
18. Hao, S. & Baltimore, D. The stability of mRNA influences the temporal order of the induction of genes encoding inflammatory molecules. *Nature Immunol.* **10,** 281–288 (2009).
19. Giorgetti, L. *et al.* Noncooperative interactions between transcription factors and clustered DNA binding sites enable graded transcriptional responses to environmental inputs. *Mol. Cell* **37,** 418–428 (2010).
20. Bhat, S., Hermann, J., Armishaw, P., Corbisier, P. & Emslie, K. R. Single molecule detection in nanofluidic digital array allows accurate measurement of DNA copy number. *Anal. Bioanal. Chem.* **394,** 457–467 (2009).
21. Wilson, J. W., Catherine, B. & Christopher, S. (eds) in *Apoptosis Genes* (Springer, 1999).
22. Lee, E. G. *et al.* Failure to regulate TNF-α-induced NF-κB and cell death responses in A20-deficient mice. *Science* **289,** 2350–2354 (2000).
23. Hutti, J. E. *et al.* IκB kinase beta phosphorylates the K63 deubiquitinase A20 to cause feedback inhibition of the NF-κB pathway. *Mol. Cell. Biol.* **27,** 7451–7461 (2007).
24. Lipniacki, T., Paszek, P., Brasier, A. R., Luxon, B. & Kimmel, M. Mathematical model of NF-κB regulatory module. *J. Theor. Biol.* **228,** 195–215 (2004).
25. Lipniacki, T., Puszynski, K., Paszek, P., Brasier, A. R. & Kimmel, M. Single TNF-α trimers mediating NF-κB activation: Stochastic robustness of NF-κB signaling. *BMC Bioinformatics* **8,** 376 (2007).
26. Delhase, M., Hayakawa, M., Chen, Y. & Karin, M. Positive and negative regulation of IκB kinase activity through IKK subunit phosphorylation. *Science* **284,** 309–313 (1998).
27. Chen, Y.-M. *et al.* Dual regulation of TNF-α induced CCL2/monocyte chemoattractant protein-1 expression in vascular smooth muscle cells by NF-κB and AP-1: modulation by type III phosphodiesterase inhibition. *J. Pharmacol. Exp. Ther.* **103,** 06262 (2004).
28. Toepke, M. W. & Beebe, D. J. PDMS absorption of small molecules and consequences in microfluidic applications. *Lab Chip* **6,** 1484–1486 (2006).

Supplementary Information is linked to the online version of the paper at www.nature.com/nature.

Acknowledgements We thank A. Leyrat and R. Gomez-Sjoberg for development of the automated cell culture system, assistance with the software, and for contributions to experimental design and preliminary data. This research was supported in part by an NIH Director's Pioneer Award (to S.R.Q.), an NCI Pathway to Independence Award (K99CA125994) (to M.W.C.), the Foundation for Polish Science (TEAM 2009-3/6) and NSF/NIH grant no. R01-GM086885 (to T.L.), a Stanford Graduate Fellowship (to T.K.L.), and a Stanford Bio-X Graduate Fellowship (to J.J.H.).

Author Contributions S.T. and J.J.H. performed the experiments, S.T. and T.L. developed the mathematical models and performed the simulations, T.K.L. developed the image processing methods and all authors contributed to analysis of the data and to writing the manuscript.

Author Information Reprints and permissions information is available at www.nature.com/reprints. The authors declare competing financial interests: details accompany the full-text HTML version of the paper at www.nature.com/nature. Readers are welcome to comment on the online version of this article at www.nature.com/nature. Correspondence and requests for materials should be addressed to M.W.C. (mcovert@stanford.edu), S.R.Q. (quake@stanford.edu) or T.L. (tlipnia@ippt.gov.pl).

METHODS

Cell lines. We previously used a lentiviral system to create $p65^{-/-}$ mouse fibroblast (3T3) cells expressing the fluorescent fusion protein p65–DsRed under control of the endogenous mouse *p65* promoter[8]. Overexpression of p65 can cause unusual NF-κB activation, and we therefore cloned the 1.5 kb upstream of the *relA* gene into the lentiviral construct to control p65–DsRed expression. We used the resulting construct to infect $p65^{-/-}$ 3T3 cells (courtesy of the D. Baltimore laboratory). These cells showed a normal response to TNF-α at the population level[8]. To relieve a bottleneck in image processing in this study, we also infected the cells with a lentivirus containing the nuclear marker H2B–GFP driven by the human ubiquitin C promoter. After cloning, the cells were frozen and newly thawed cells were used for each experiment to prevent 3T3 cell re-transformation and to minimize heterogeneity. A correlation between p65–DsRed levels and cell activation was not observed[8].

Microfluidic cell culture experiments. Cells were seeded at constant density around 20,000 cells cm^{-2} (200 ± 25 cells per chamber) into microfluidic chambers and were cultured for one day to reach near 50% confluence before stimulation experiments. The external conditions were set to standard culture conditions (5% CO_2 and 37 °C external temperature) and maintained at this level. During cell growth, 33% of the chamber volume was replaced with fresh media (DMEM) every hour using the nanolitre microfluidic pump, which resulted in vigorous proliferation of 3T3 cells. We made sure that cells were healthy, motile and proliferating before TNF-α stimulation experiments. We were able to establish such cultures for durations up to a week in the microfluidic chambers, depending on initial seeding density. During stimulation experiments, various TNF-α (Roche) dilutions in DMEM were kept on ice at all times and the fluids were flowed quickly into the microfluidic chambers during stimulation to avoid degradation of TNF-α. The high surface-area to volume ratio of the plastic tubing and the microfluidic environment we used allow rapid warming of the media when it enters the environmental chamber, therefore the media flown in the chambers were at ambient (37 °C) temperature. The media and TNF-α vials were pressurized with 5% CO_2 to minimize pH change. Cell viability was not affected negatively during media flow and stimulation. The microfluidic culture chip[3] allows the replacement of the entire culture media in less than a second, which results in a step-like TNF-α concentration profile on the timescales of NF-κB dynamics. Once the TNF-α loaded media was flowed in, the chambers were sealed and were imaged every 6 min in both GFP and dsRed fluorescence channels during the entire experiment, for up to 12 h. The cells were not fed with media after stimulation and during imaging; they remained in the same TNF-α loaded media during the entire experiment without disturbance. All TNF-α concentrations (up to ten at a time) were tested in parallel chambers (with duplicates) in a single experiment, and such experiments were repeated multiple times with minimal variation between results. We therefore tested up to 20 different microfluidic chambers at a time. We have not observed any negative effect due to TNF-α adsorption into PDMS-based microfluidics, although absorption into PDMS needs to be taken into account when small, hydrophobic molecules are used[28].

Image acquisition and quantification. Cells were imaged in both the GFP and DsRed channels with a Leica DMI6000B microscope (20× air objective) and Retiga-SRV CCD camera (Q Imaging) every 5–6 min for several hours. Cell traces were visually checked and compared to images to exclude mitotic cells, as mitotic cells typically show increased signal intensity that could be confused with active cells. The fraction of responding cells at each concentration was calculated as the number of responding cells divided by the sum of responding and non-responding cells. To generate time courses of NF-κB localization in single cells, custom Matlab software using the Image Processing Toolbox was used to automatically identify the nuclei from H2B–GFP images and extract nuclear intensities from p65–DsRed images. To identify nuclear regions, H2B–GFP images were local range contrast filtered with a neighbourhood of three pixels and then thresholded, where the threshold level was automatically determined by *k*-means clustering pixel intensities with $k = 3$. Touching or merged nuclei (determined by solidity <0.925) were then separated by a watershed transform with markers seeded at *k*-means clustered centroids. Nuclei between time points were then linked to the nearest nuclei in the next time point and preliminary quality control checked for constant nuclear area through tracking. H2B–GFP and p65–DsRed images were aligned by cross-correlation when necessary and nuclear intensities were then extracted from the associated p65–DsRed image. For the first time point, cytoplasmic areas and p65–DsRed intensities were extracted through a combination of local thresholding and watershed transforms with the nuclei as marker seeds. All cell tracking was manually checked to eliminate mistakes by the automated analysis. Cells that divided or left the field of view during the experiment were not included in the analysis of NF-κB localization dynamics. Time courses of NF-κB localization were linked to the responding or non-responding classification using the XY coordinates in the field of view. The mspeaks function in the Bioinformatics Toolbox of Matlab was used to identify peaks in NF-κB nuclear localization and to calculate the times of full-width half maximum of the first peak. Localization dynamics from cells that were judged to be non-responders were used to determine a peak threshold for responding cells. Because we could not always image the ascending portion of the first peak with sufficient temporal resolution, we calculated the difference between the time of the first peak (response time) and the later full-width half maximum time, which we called the first peak decay time. Subsequent statistical analysis was performed with Matlab.

Nuclear localization peak intensity, timing and area. The peak intensity and timings of the peaks were found using custom peak detection software written in Matlab. The area under each nuclear localization peak is a measure of the total NF-κB nuclear activity that lead to the transcription of target genes (that is, the total amount and duration of NF-κB presence in the nucleus), whereas the peak intensity is a measure of the maximum level of the transcriptional activity. At each dose, the area of the first peak was integrated from the time of TNF-α stimulation to the first minimum for each cell using Matlab. The delayed rise time observed during low-dose stimulation results in increased peak width, which compensates the reduced peak intensity, resulting in nearly equal mean first-peak areas at all doses.

Gene expression measurements. Cells cultured in well plates were stimulated with six different TNF-α concentrations from 0.01 ng ml^{-1} to 10 ng ml^{-1} prepared in DMEM media. At the end of each stimulation experiment (0.25, 0.5, 2, 4, 6, 8, 10 and 12 h after stimulation), cells were lysed and cDNA was synthesized using Cells Direct One Step RT–PCR kit (Invitrogen), and TaqMan primers and probes (Applied Biosystems) were used for real-time qPCR. These were population-based measurements, with nearly 500 cells in each qPCR reaction, containing both active and non-active cells. Each experimental condition had quadruple replicates, and was compared to control wells where cells were not stimulated with TNF-α. Each condition was measured at least three times. We used microfluidic dynamic arrays (Fluidigm 48x48 Dynamic Array) to perform 2,304 qPCR reactions in parallel, and all 64 × 24 experiments (×4 replicates of each reaction) consumed three dynamic arrays. The cycle thresholds (C_T) (Supplementary Table 2) measured during qPCR reactions were converted into relative expression levels (2^{-C_T}). The relative gene expression levels were then calibrated for total mRNA molecules per cell via digital-PCR measurements performed on a single gene (Fluidigm 12 Digital PCR Chip)[20]. Figure 2a shows mRNA levels measured on populations that contain active and non-active cells, and includes the baseline (no TNF-α) level expression. In Fig. 2b, c, we estimate the mRNA levels for only active cells, by first subtracting the baseline level, and then dividing the differential expression levels with the fraction of active cells at each dose measured in Fig. 1, and finally calibrating using digital-PCR measurements. Figure 2b shows that early genes are expressed at very high levels in active cells even at the lowest TNF-α doses, demonstrating how single-cell data can be used to interpret population-based measurements of gene expression.